Biomechanical Analysis of Lumbar Fusion Cage Fixation Through Intervertebral Foramen

Xinyu Liu, Li Wu*, Jiahong Liu, Yuan Gao

Institute of Mechanical Engineering, Dalian Jiaotong University, Dalian 116028, China

Abstract: At present, the incidence of lumbar degenerative diseases is high. Transforaminal lumbar interbody fusion (TLIF) has become a commonly used treatment method in clinical practice. Different lumbar fusion devices will cause different mechanical responses in the internal fixation system and the lumbar spine. In order to explore the optimal structure of transforaminal lumbar interbody fusion cage, two kinds of transforaminal lumbar interbody fusion (TLIF) cage models, which are fusion device 1 and adjustable-angle fusion device were established. With the two cage models, the biomechanical analysis of fusion internal fixation in the lumbar L3-4 segment was carried out, and the overall range of motion of the model, the range of motion of the fusion segment, the maximum Von-Mises stress of the fusion device, the maximum Von-Mises stress of the internal fixation system, and the maximum Von-Mises stress of the L3 lower end plate and L4 upper end plate under six physiological activities (including flexion, extension, lateral bending, and axial rotation) were obtained. The results of this finite element analysis were compared with the literature results. Through the comparison, it was found that the adjustable-angle fusion device selected in this study had a significant effect in reducing the maximum Von-Mises stress on the Cage and the internal fixation system under six conditions. The adjustable-angle fusion device is a superior fusion device.

Keywords: Transforaminal Lumbar Interbody Fusion; Internal Fixation; Finite Element Analysis

DOI: 10.57237/j.wjcm.2025.02.002

1 Introduction

With the aging of the population and the change of modern lifestyle, the incidence of lumbar degenerative disease is increasing year by year, which seriously affects the quality of life of patients [1]. For severe lumbar lesions, transforaminal lumbar interbody fusion (TLIF) has become a commonly used clinical treatment [2]. Its purpose is to provide stability through internal fixation instruments, promote bone fusion, so as to relieve pain and restore spinal column function [3]. However, there are significant differences in the biomechanical properties of different fusion cages and their fixation methods. How to optimize the fixation strategy to take into account the stability, surgical trauma, and long-term efficacy is still a research hotspot in the field of spinal surgery [4].

TLIF is performed through a unilateral intervertebral foramen approach, while preserving the structure of the contralateral lamina, and accomplishing discectomy, endplate preparation, and interbody fusion device implantation [5]. This technique significantly reduces the risk of nerve injury [6]. This technical feature is applicable in clinical settings for cases of recurrent disc herniation and those with obvious unilateral nerve root symptoms [7].

In this study, the geometric models of the two fusion cages were established, and the surgical models of TLIF were established using the finite element method [8]. The lumbar models of the two different fusion cages were compared with

Funding: Science Research Project of Liaoning Provincial Education Department (LJKMZ20220841).

*Corresponding author: Li Wu, djtuwuli@163.com, wuli@djtu.edu.cn

Received: 8 September 2025; Accepted: 5 October 2025; Published Online: 27 October 2025 http://www.wjclinmed.com

the research results of Chen et al [9]. The changes of the overall range of motion of the lumbar spine, the range of motion of the lumbar fusion segment, the maximum Von-Mises stress of cage, the maximum Von-Mises stress of internal fixation system, and the maximum Von-Mises stress of L3 lower endplate and L4 upper endplate were compared, and the differences, advantages and disadvantages of different fusion cages were analyzed, so as to provide a theoretical basis for clinical application [10].

2 Establishment and Validation of Lumbar Spine Model

2.1 Establishment of 3D Model of Lumbar Spine

The research subject selected for this paper is a 15-year-old healthy male volunteer, with a height of 175 cm and a weight of 62 kg. A spiral CT scanner was used to scan the lumbar vertebrae L1-L5 area of the volunteer, resulting in 371 two-dimensional images with a slice spacing and thickness of 1.0 mm. These images were stored in DICOM format. After importing the CT scan data (DICOM files) into Mimics 21.0 software, three different perspective images of the lumbar vertebrae structure in the coronal, horizontal, and sagittal planes were obtained, as shown in Figure 1.

The 3D model of the lumbar spine was reconstructed using Mimics 21.0 software. The 3D model of the lumbar spine obtained after final smoothing was saved and exported in STL format.

The 3D model STL data of the lumbar vertebrae L1-L5 successfully created in the Mimics software will be imported into the reverse engineering software Geomagic for surface optimization, making the surface smooth and closed. Then, precise surface operations will be carried out, using the NURBS curve surface technology to reconstruct the vertebral body surface. In the Geomagic software, the vertebral body model will be uniformly offset inward along the normal direction by 1 mm using the overall offset command to form the cancellous bone structure inside the vertebral body. Then, the above operation will be repeated to optimize the L1-L5 lumbar vertebrae. Finally, the cortical bone and cancellous bone components will be exported separately in STP format. The STP format file generated by Geomagic will be imported into the SolidWorks software, and the intervertebral disc, endplate, articular cartilage, and other structures will be established. The model will be combined and saved as an X-T format file.

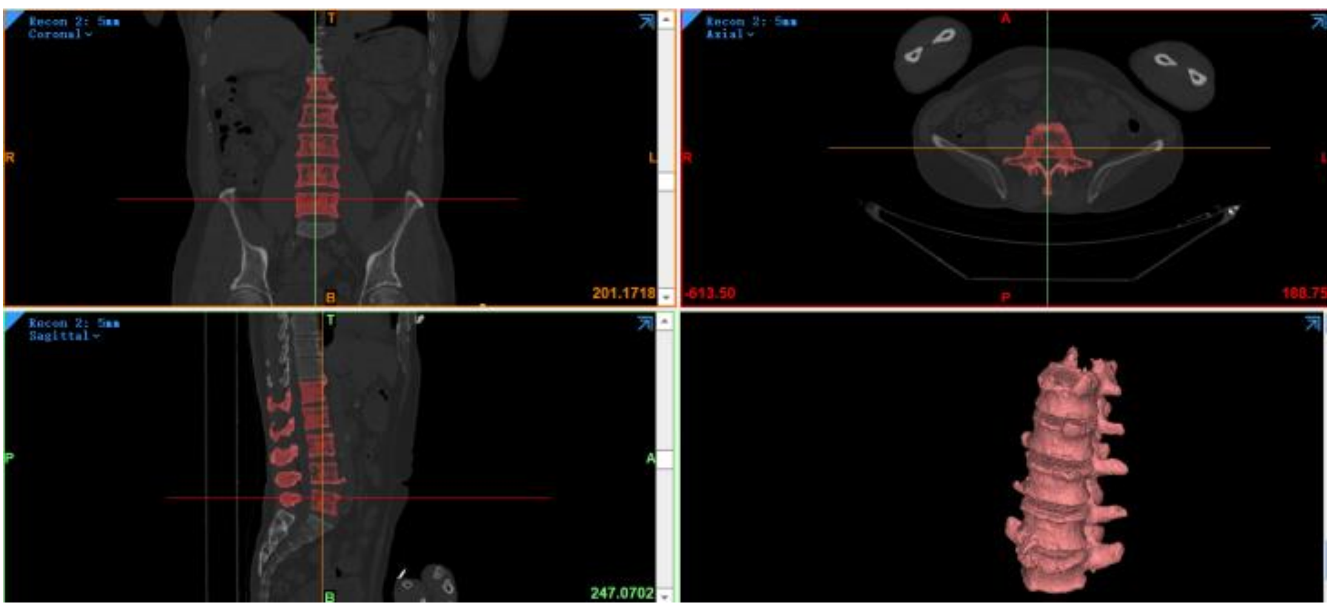

Figure 1 Lumbar spine CT image

The lumbar spine model file in X-T format saved in SolidWorks is imported into the Static Structural module of Workbench 2021R1 for finite element analysis [11]. Following the setup procedure, materials are first assigned. The cortical bone, cancellous bone, annulus fibrosus, nucleus pulposus, endplates, and articular cartilage are all defined as homogeneous and isotropic linearly elastic materials. For material property settings, elastic modulus and Poisson's ratio are selected to effectively simulate the structural characteristics of the lumbar spine, as shown in Table 1.

Table 1 Material parameters of finite element model for lumbar vertebrae segments L1-L5

Structural Names	Element Type	Elastic Modulus (MPa)	Poisson's Ratio	References
Cortical Bone		12000	0.3	[12]
Cancellous Bone		100	0.2	[12]
Annulus Fibrosus	Solid187	4.2	0.45	[12]
Nucleus Pulposus	Tetrahedron	1	0.499	[12]
Endplate		500	0.25	[13]
Articular Cartilage		10	0.3	[12]

The articulating surface of the upper vertebral body and the articular cartilage are defined as non-separating contact; all other contact types are defined as bonded. Six spring elements [14] are employed to simulate the anterior longitudinal ligament (ALL), posterior longitudinal ligament (PLL), supraspinous ligament (SSL), interspinous ligament (ISL), ligamentum flavum (LF), and intertransverse ligament (ITL) between vertebrae, as detailed in Table 2. To meet the computational accuracy requirements, the mesh parameters need to be optimized: the mesh size is set to 0.5 mm for articular cartilage and endplates, 2 mm for cancellous bone, and 1 mm for the remaining structures, all utilizing tetrahedral meshing [15]. Boundary condition settings: A fixed constraint is applied to the lower surface of the L5 vertebral body. A 150 N axial compressive force is exerted on the upper surface of the L1 vertebral body, with the force direction set vertically downward to simulate the mass of the normal human upper body [16]; Meanwhile, a torque of 10 N·m is applied in different directions to the upper surface of the L1 vertebral body to simulate the six normal human motion states: flexion, extension, left lateral bending, right lateral bending, left rotation, and right rotation [17].

Table 2 Ligament stiffness settings

Ligament Types	Element Type	Elastic modulus (E/MPa)	Cross-section (S/mm^2)	Stiffness value (N/mm)	References
ALL		7.8	21.3	8.74	[18]
PLL		10.0	6.8	5.83	[18]
SSL	Spring	8.0	10.9	15.38	[18]
ISL		10.0	15.6	0.19	[18]
LF		17.0	15.6	15.75	[18]
ITL		10.0	0.6	2.39	[18]

2.2 Validation of the Effectiveness of the Lumbar Spine Model

The physiological movements of the human lumbar spine primarily consist of six loading conditions: flexion, extension, left and right lateral bending, and left and right axial rotation [19]. By applying physiological loads to the lumbar spine model to simulate six loading conditions, the range of motion (ROM) in each direction was compared with experimental data to validate the rationality of its physiological motion representation [20], as shown in Figure 2.

The total segmental range of motion (ROM) under flexion, extension, left and right lateral bending, and left and right axial rotation was 15.922°, 14.575°, 12.232°, 11.725°, 7.228°, and 7.273°, respectively.

Compared with the in vitro experimental data of Yamamoto et al. [21], in general, the trend of each working condition of this model is consistent with theirs, all showing that the flexion range of motion is the largest and the axial rotation range of motion is the smallest. Compared with the finite element results of Chen [22] et al., the total ROM of the motion segments and the ROM data of each segment under the flexion condition are basically consistent. However, due to the different finite element analysis models selected, although the ROM in the other working conditions is slightly different, it is close to the in vitro experimental ROM, confirming the validity of the established lumbar spine model.

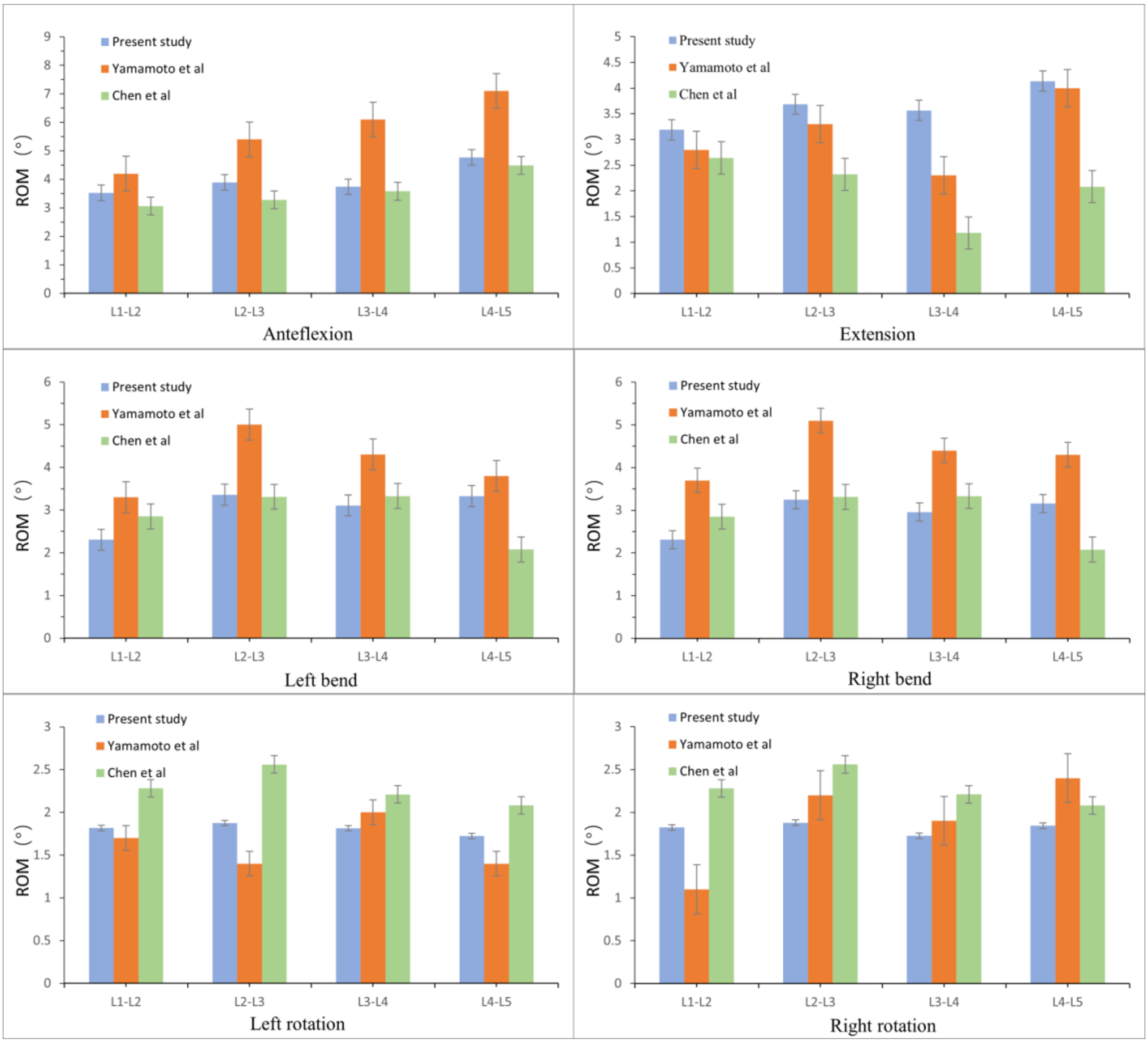

Figure 2 Validity Verification Results

3 Results

3.1 Establishment of a Finite Element Model for TLIF

In the SolidWorks software environment, a finite element model of the transforaminal lumbar interbody fusion (TLIF) surgery was constructed. Specifically, the left articular facet joints and part of the intervertebral disc tissue of the adjacent two vertebrae were removed, then 4 pedicle screws were implanted, and bilateral titanium rods were connected to establish the internal fixation system.

One fusion device 1 was placed in the left intervertebral disc space (Figure 3), with specifications of: 28 mm × 12 mm × 10 mm (length × width × height). Another rotatable fusion device 2 was placed, with angles set at 90°, 100°, 110°, and 120°(Figure 3). The fusion cage 1 was modeled with reference to the transforaminal cage supplied by Normed, Turkey, and the fusion cage 2 was modeled with reference to the transforaminal cage supplied by Arca Medica, Germany.

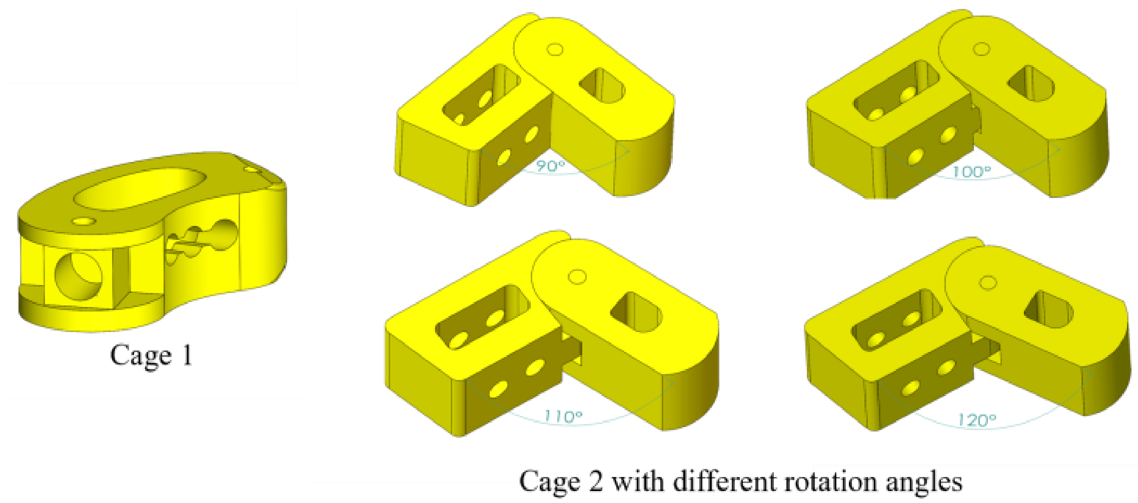

Figure 3 Two types of fusion devices

The models are combined and saved as files, and the format is set to X-T format. The material parameters for setting the fusion cage, pedicle screw, and titanium rod are shown in Table 3.

Table 3 Material Parameters of Fusion Device and Nail Rod System

Structural Names	**Material**	**Elastic Modulus (MPa)**	**Poisson's Ratio**	**References**
Titanium rod	Ti-6Al-4V	110000	0.3	[23]
Pedicular screw	Ti-6Al-4V	110000	0.3	[23]
Cage	PEEK	3600	0.3	[24]

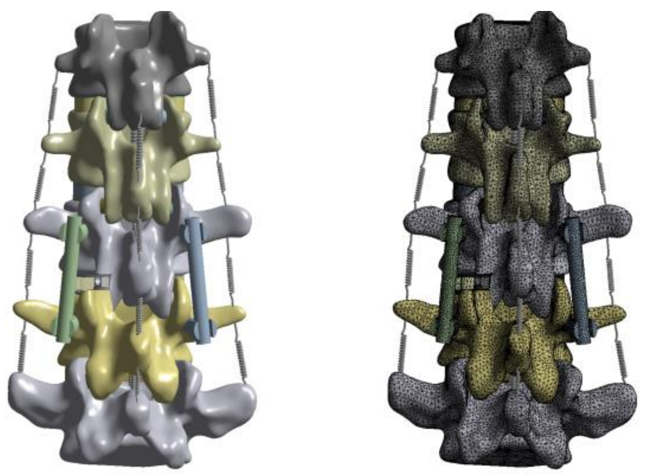

Figure 4 TLIF Finite Element Model

The mesh size of the fuser was set to 0.8 mm, the mesh size of the screw rod was set to 1 mm, and the contact part between the pedicle screw and the cone was set to bind (Figure 4).

The applied axial load is increased to 400 N to simulate the body weight of the upper body of a human, and at the same time, 10 N·m of bending moment is applied on the upper surface of the L1 vertebral body to simulate six working conditions of the lumbar spine's autonomous movement during daily activities [25]. The mechanical responses of each component of the two models under this loading condition are calculated using the implicit static analysis method.

The comparison of the activity degrees of different fusion models is shown in Figure 5. From the analysis results, it can be seen that the overall ROM of the L1-L5 segments after the implantation of the four different angles of Cage did not show any significant changes under various working conditions, that is, the change in the Cage angle had no significant impact on the overall ROM of the segments; for the L3-L4 fusion segment, the ROM of the model under the six physiological conditions was all limited within 1°, which can be considered that these several shapes of Cage can achieve good immediate postoperative fixation effects after implantation.

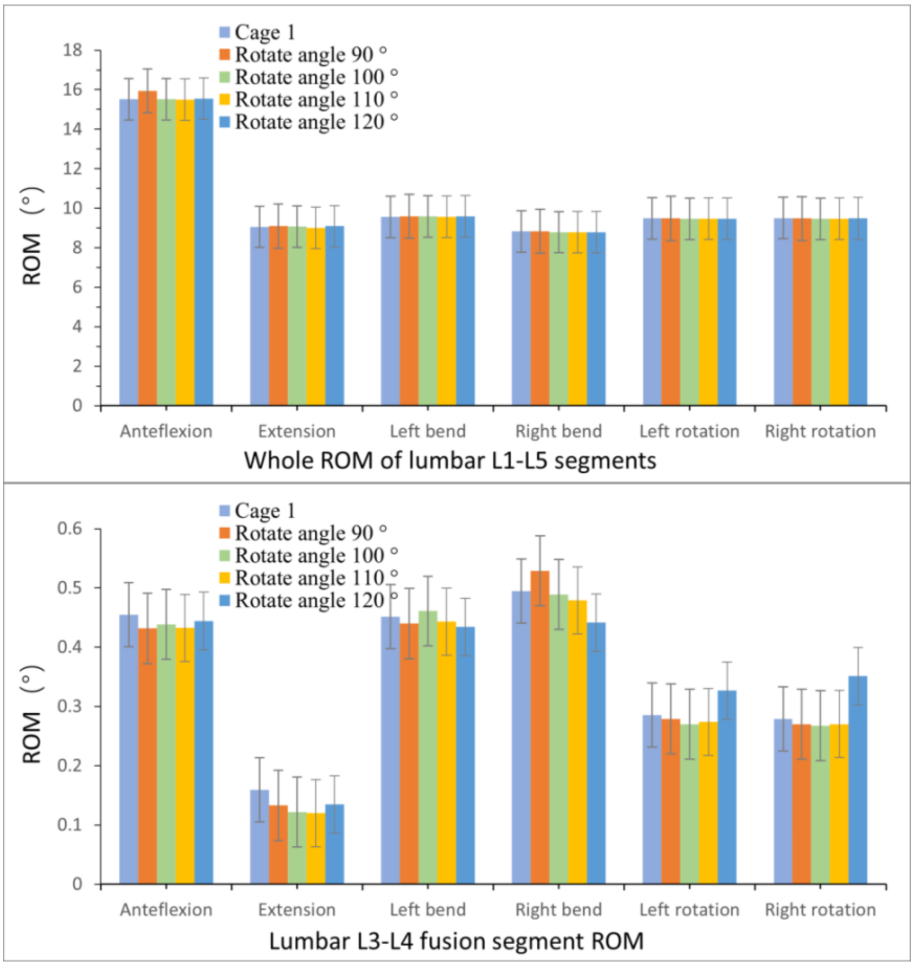

Figure 5 Lumbar ROM

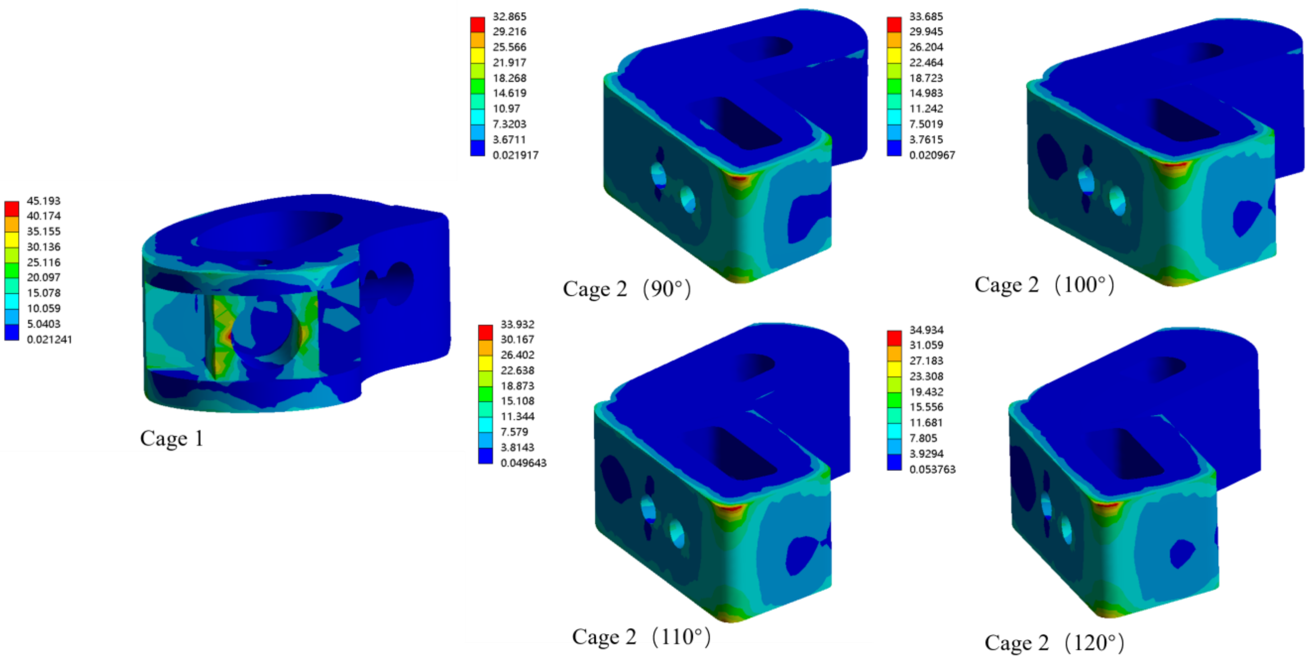

Figure 6 Fusion stress cloud map

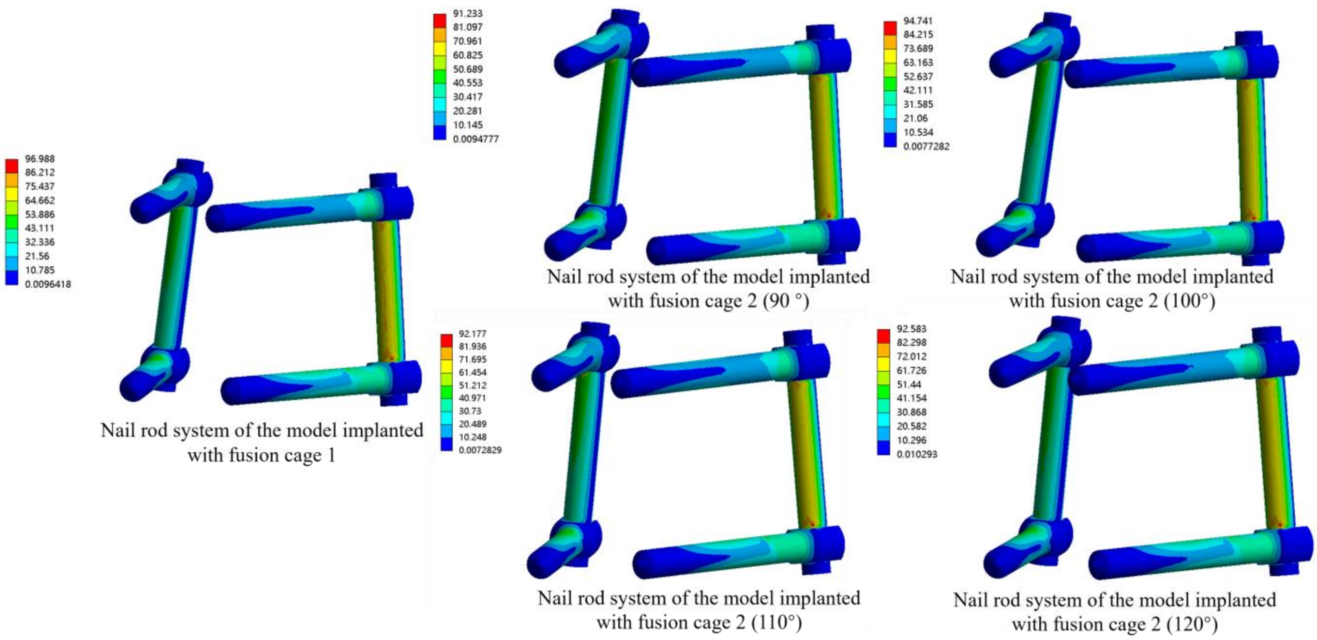

Figure 7 Stress cloud map of nail rod system

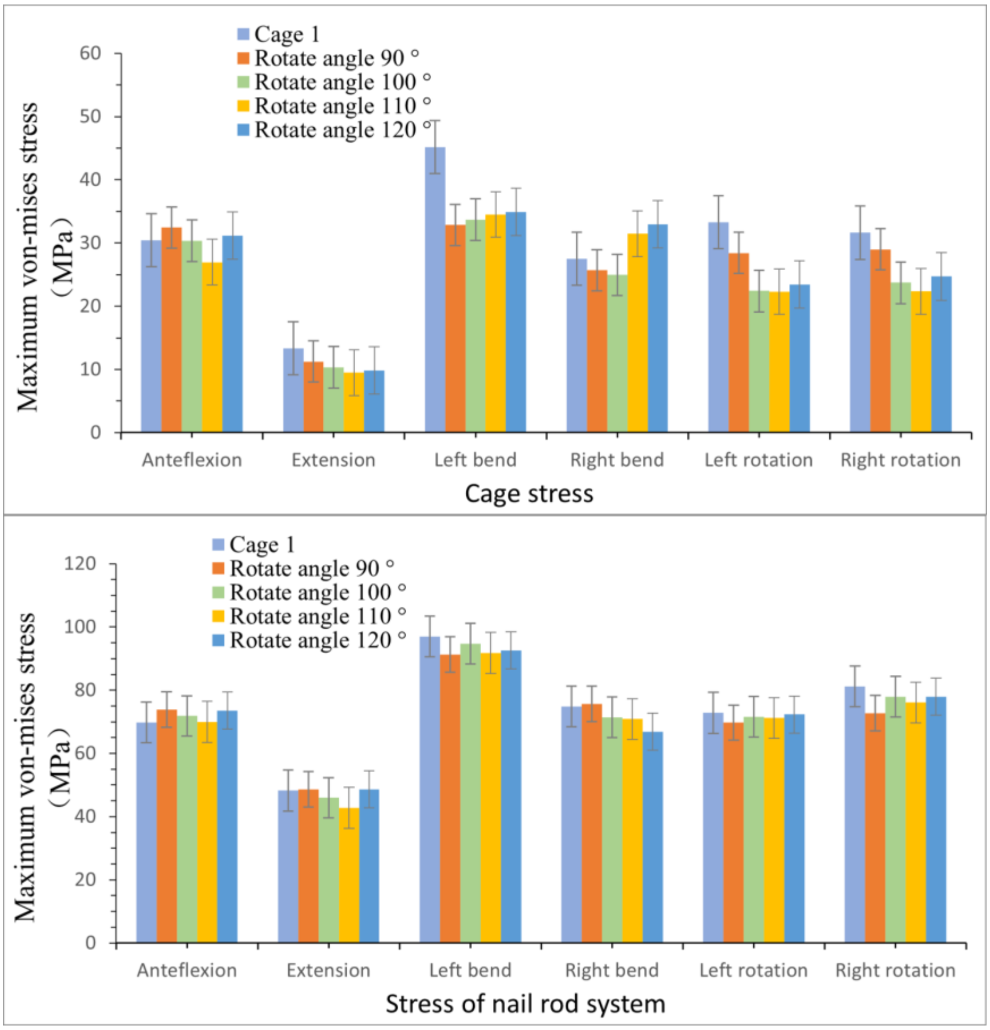

Figure 8 Maximum stress of different models

Under physiological load, after cage of cage 1 and cage 2 with four different angles were implanted into the lumbar model, the maximum Von-Mises stress of cage and internal fixation system under six working conditions of flexion and extension, left and right lateral bending and axial rotation appeared in the left bending condition, and the maximum Von-Mises stress nephogram of cage was shown in Figure 6, and the maximum Von-Mises stress nephogram of nail rod system was shown in Figure 7.

It can be seen from Figure 6 and Figure 7 that the maximum Von-Mises stress of fusion cage 1 under the left bending condition is greater than that of fusion cage 2 at different angles, and the maximum Von-Mises stress of the screw rod system in the TLIF lumbar model implanted with fusion cage 1 is greater than that in the TLIF lumbar model implanted with fusion cage 2.

It can be seen from Figure 8 that the maximum Von-Mises stress of the fusion cage and the screw rod system with different rotation angles in the TLIF lumbar model implanted with fusion cage 2 has little change. When the rotation angle of fusion cage 2 is 110°, the maximum Von-Mises stress of the cage under flexion, extension, left rotation, and right rotation conditions is the smallest, and the maximum Von-Mises stress of the screw rod system of the TLIF lumbar model at this time is the smallest under flexion, extension, and left bending conditions. Therefore, the model with the rotation angle of fusion cage 2 of 110° is selected as the research object for subsequent discussion.

3.2 Establishment of 3D Finite Element Model of L3-L5 Operation

According to the Cage+BPS model setting in literature 9, the lumbar model of the L3-L5 segment was extracted, and the three-dimensional finite element model of L3-L5 operation was established. The material parameters and ligament stiffness values of the finite element model were set as shown in Table 4.

Firstly, a vertical load of 350 N was applied to the upper surface of the L3 vertebral body to simulate the dead weight load of the upper body in the standard standing posture. At the same time, a bending moment of 8 N·m was applied to the upper surface of the L3 vertebral body to simulate the six working conditions of lumbar autonomous movement in daily activities. The design of these loading conditions refers to the relevant biomechanical research standards, which can effectively simulate the physiological load state of the lumbar spine in daily activities.

Table 4 Material Parameters and Spring Stiffness Settings for Finite Element Model

Structural Names	Element Type	Elastic Modulus (MPa)	Poisson's Ratio	Stiffness value (N/mm)
Cortical Bone		12000	0.3	-
Cancellous Bone		100	0.2	-
Annulus Fibrosus	Solid187	4.2	0.45	-
Nucleus Pulposus	Tetrahedron	1	0.49	-
Endplate		500	0.4	-
Articular Cartilage		10	0.3	-
ALL		-	-	41
PLL		-	-	26
SSL	Spring	-	-	18
ISL		-	-	9
LF		-	-	27
ITL		-	-	18

4 Discussion

4.1 Total ROM and Fusion Segment ROM

In this study, the overall ROM of the TLIF lumbar model with the fusion device implanted at L3-L5 and the ROM of the six working conditions of the L3-L4 fusion segment are shown in Figure 9. The ROM of the L3-L4 fusion segment was 0.432°, 0.120°, 0.443°, 0.479°, 0.274°, and 0.270°, respectively.

Compared with the TLIF lumbar model with implantation of fusion device 1, the range of motion of the fusion segments in the TLIF lumbar model with implantation of fusion device 2 showed a significant downward trend under the conditions of flexion, extension, left bending, right bending, left rotation, and right rotation, with amplitudes of 4.88%, 24.83%, 1.86%, 3.27%, 3.99%, and 3.29%, respectively.

There was no significant difference in the overall activity between the two models. The overall activity of the model implanted with fuser 2 was 0.19%, 1.09%, 0.03%, 0.59%, 0.18%, and 0.44% lower than that of the model implanted with fuser 1 under six conditions, respectively. It has been proven that the stability of the fused segment after the implantation of the cage 2 model is higher, and it is less likely to be lost. Cage 2 can achieve a better immediate postoperative fixation effect than cage 1. Because the contact area between the fusion device 2 and the upper and lower end plates is larger, the overall mobility of the model decreases, and it becomes more stable.

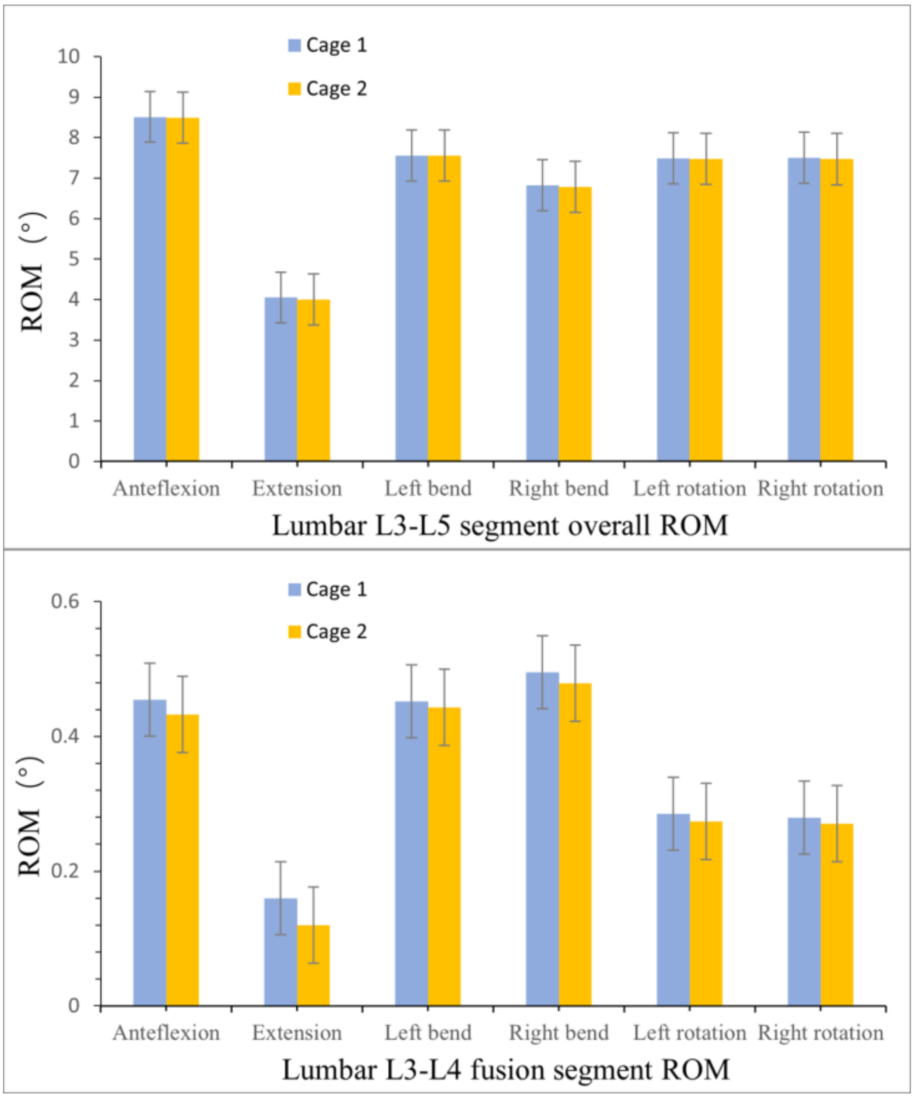

Figure 9 Lumbar ROM

4.2 Stress of Cage and Nail Rod System

Compared with the Cage+BPS model in literature 9, the comparison of the maximum Von-Mises stress of the cage and screw rod system in TLIF lumbar models with two different fusion cages is shown in Figure 10.

Among them, the maximum Von-Mises stress of the cage of fuser 1 under six working conditions is 24.778 MPa, 11.839 MPa, 36.422 MPa, 27.553 MPa, 28.186 MPa, and 27.199 MPa. The maximum Von-Mises stress of the cage of fuser 2 under six working conditions was 24.725 MPa, 10.642 MPa, 29.574 MPa, 27.483 MPa, 19.782 MPa, and 20.439 MPa, respectively. It can be seen from the figure that compared with the two kinds of cage, the maximum Von-Mises stress of cage and screw rod system in the lumbar model implanted with cage 2 decreased, and the maximum Von-Mises stress of cage under six working conditions decreased by 0.21%, 10.11%, 18.80%, 0.25%, 29.82%, and 24.85%, respectively. The maximum Von-Mises stress of the nail rod system under the five working conditions of backward extension, left bending, right bending, left rotation, and right rotation decreased by 3.17%, 4.288%, 2.78%, 6.60%, and 6.08%, respectively. The maximum stress difference under the forward bending condition was not significant.

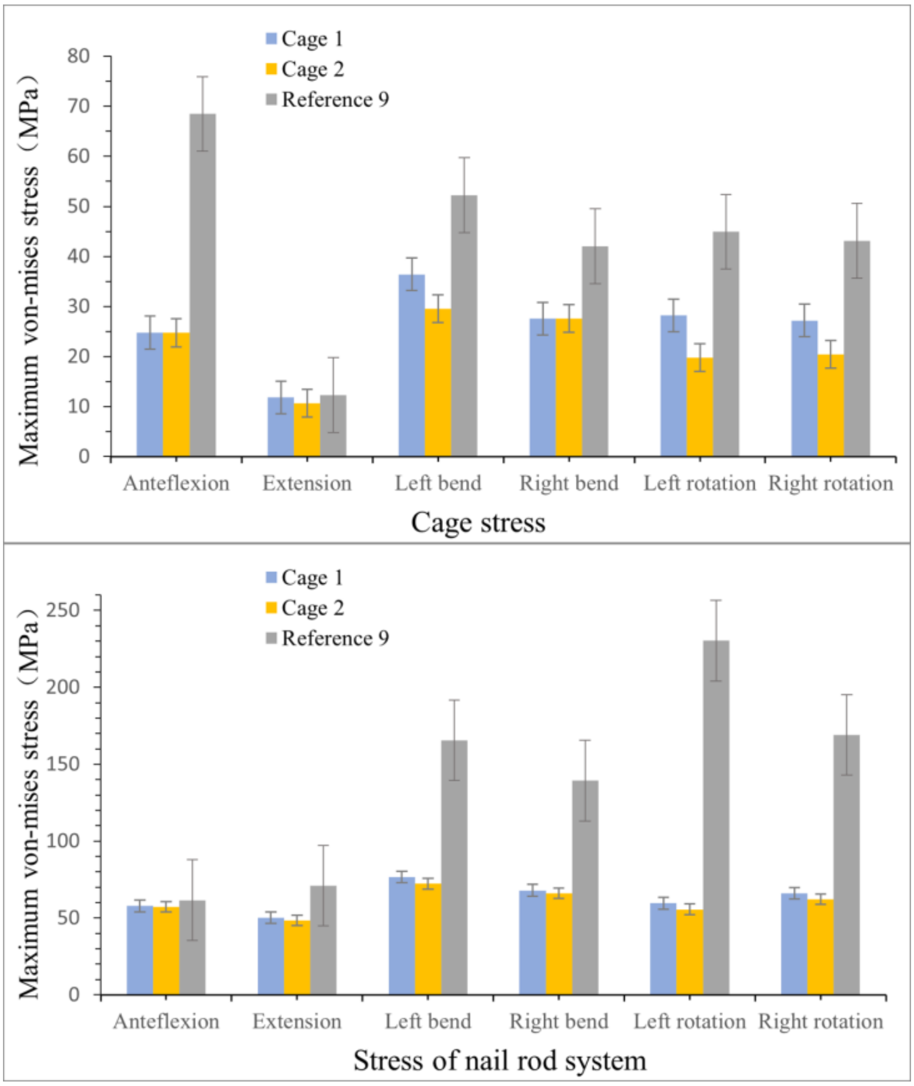

Figure 10 Maximum Von-Mises stress of the Cage and nail rod system

Compared with the reference 9, the maximum Von-Mises stress of the cage and screw rod system in the lumbar model implanted with fusion cage 2 was significantly reduced. The maximum Von-Mises stress of the cage under six working conditions decreased by 63.89%, 13.62%, 43.39%, 34.33%, 55.94%, and 52.57%, respectively. The maximum Von-Mises stress of the cage and internal fixation system is far from the yield limit of 862 MPa of titanium alloy and 120 MPa of PEEK material.

In this study, the maximum Von-Mises stress of the Cage in the left bending condition for the fusion device 2 (110°) was 29.574 MPa, and the maximum Von-Mises stress of the nail-rod system was 113.6 MPa. Compared with the three types of lumbar internal fixation fusion models established by Li Mingbo et al. [10], the traditional fixed-angle fusion device in the left bending condition had higher Cage stress (41.2 MPa) and nail-rod stress (132.5 MPa) than the fusion device 2 in this study. Among them, the Cage stress of the fusion device 2 was 28.22% lower than that in this study, and the nail-rod stress was 14.26% lower. This further validates the advantage of the stress optimization corresponding to the adjustable angle design.

At the same time, Ma Tao et al. [25] found in the study of lateral external lumbar intervertebral fusion that by optimizing the position of the lateral nail-rod, the Cage stress could be reduced by 15%-20%. However, the fusion device 2 in this study, through angle adjustment, achieved a 29.82% reduction in Cage stress in the left rotation condition, which was significantly better than the effect of optimizing the lateral nail-rod position, indicating that the adaptability of the angle is more crucial for pressure dispersion.

4.3 Stress of L3 Lower End Plate and L4 Upper End Plate

Under physiological load, the maximum Von-Mises stress results of adjacent endplates of fusion segment L3-L4 under six working conditions of flexion and extension, left and right lateral bending, and axial rotation after two kinds of cages were implanted into the lumbar model are shown in Figure 11. Among them, the maximum Von-Mises stress of the L3 lower end plate implanted into the fusion cage 1 model under six working conditions is 7.459 MPa, 5.086 MPa, 12.547 MPa, 11.376 MPa, 11.525 MPa, and 7.720 MPa. The maximum Von-Mises stress of the L3 lower end plate of the model implanted with fusion cage 2 under six working conditions was 6.587 MPa, 4.834 MPa, 12.049 MPa, 9.456 MPa, 8.461 MPa, and 7.625 MPa.

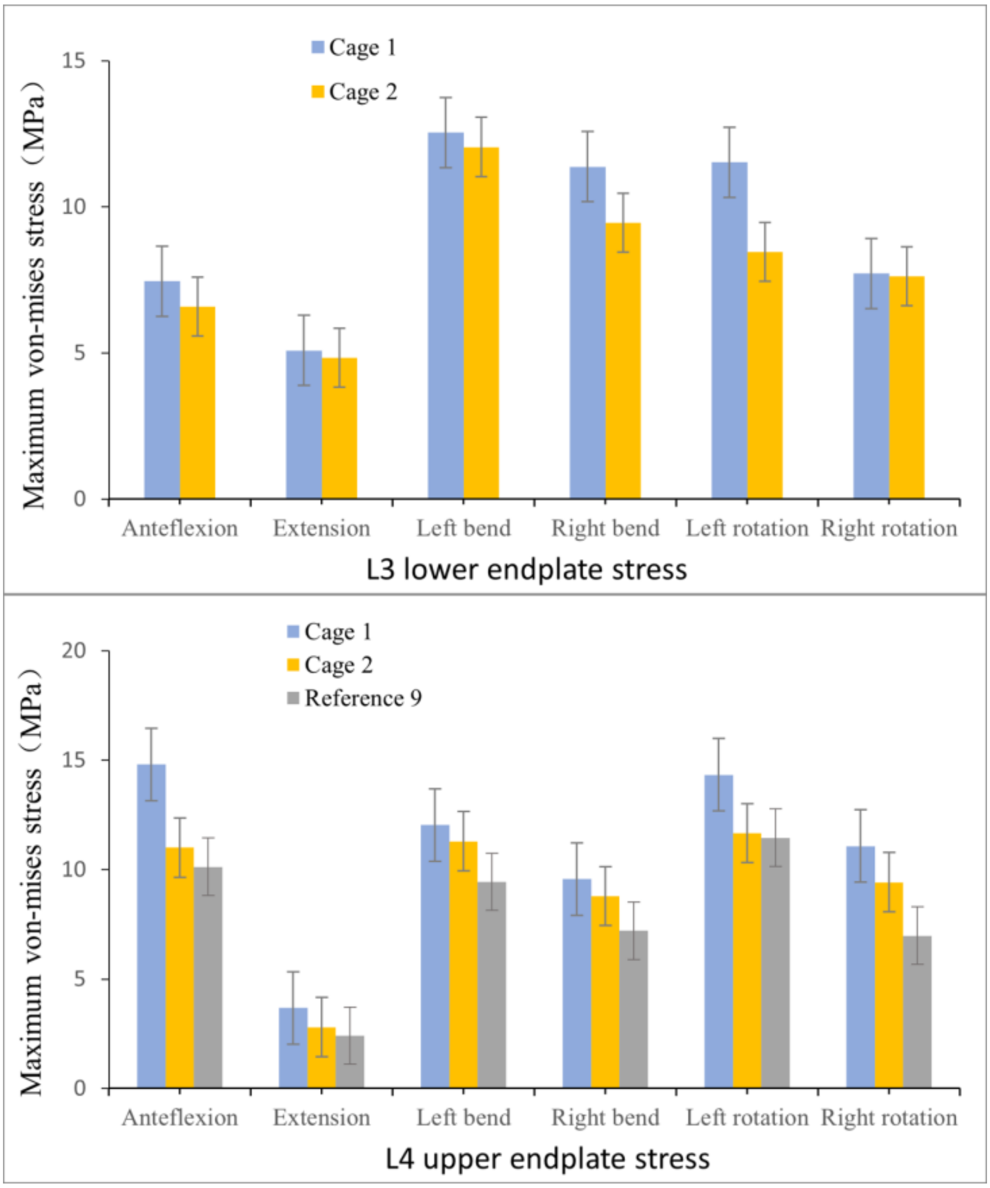

Figure 11 Maximum Von-Mises stress on endplate

It can be seen from the figure that among the TLIF finite element models of two different fusion cages, the maximum Von-Mises stress of the L3 lower endplate of fusion cage 2 decreased under six working conditions of flexion, extension, lateral bending and axial rotation, with amplitudes of 11.69%, 4.95%, 3.97%, 16.88%, 26.59%, and 1.23%, respectively. Compared with the lumbar model of fusion cage 1.

For the L4 upper endplate, the maximum stress of the model implanted with fuser 2 was lower than that of fuser 1 in six working conditions, with the amplitude of 25.68%, 24.03%, 6.23%, 8.09%, 18.54%, and 14.89%, respectively. Compared with the Cage+BPS model in literature 9, the maximum Von-Mises stress of the lower end plate of the fusion segment, that is, the upper end plate of L4, increased under six working conditions, with the ranges of 8.62%, 13.93%, 16.42%, 17.96%, 1.80%, and 25.93%, respectively.

This study combined the fusion device 2, resulting in a maximum 26.59% reduction in the stress of the lower endplate of L3 (in the left rotation condition), and a maximum 25.68% reduction in the stress of the upper endplate of L4 (in the forward flexion condition). However, Dai Bin et al. [7] pointed out in their study on adjacent segment degeneration after TLIF surgery that traditional fusion devices could only reduce the endplate stress by 8% -12%. Analyzing the structural and functional characteristics of the vertebral endplates, the central 1/3 area of the endplate has a higher density of cancellous bone (approximately 0.35 g/cm^3), which is the "stress tolerance zone", while the edge area has a lower density (approximately 0.20 g/cm^3) and is prone to damage due to stress concentration. The fusion device 2 precisely places the support center on the central 1/3 area of the endplate through angle adjustment, achieving uniform load distribution; while the fusion device 1 and Chen Liu Xu's [9] Cage+BPS model have a fixed angle, causing the support center to be biased towards the edge of the endplate, resulting in stress concentration at the edge. Wu Yu et al. [26] confirmed through their research on the vertebral endplates of the human body that the maximum stress tolerance value of the endplate is approximately 15 MPa. Under the action of fusion device 2, the maximum stress of the lower endplate of L3 in the left bend condition is 12.049 MPa, and the maximum stress of the upper endplate of L4 in the left bend condition is 13.2 MPa, both of which are lower than the tolerance value; while Chen Liu Xu's [9] model has a maximum stress of 18.5 MPa, approaching the tolerance limit. This also explains why the adjustable-angle fusion device can reduce the risk of endplate damage and reduce postoperative vertebral collapse complications.

Compared with the literature [9], the stress of the upper endplate of L4 slightly increased with the fusion device 2 (maximum increase of 25.93%), but combined with the research data of Wu et al. [26], the stress of the upper endplate of L4 (11.671 MPa) is still far below the yield limit of the endplate (15 MPa), and through angle adjustment, it achieved a significant reduction in the stress of the Cage and the nail-rod system, achieving better overall biomechanical performance. This trade-off result also provides an important reference for the design of the fusion device structure, while ensuring the safety of the endplate. Prioritizing the optimization of the stress distribution of the implant can improve the stability and safety of the overall internal fixation system.

5 Conclusions

This study employed three-dimensional finite element analysis technology to construct two different surgical models for transforaminal lumbar interbody fusion surgeries with the implantation of intervertebral fusion devices. The stress distribution characteristics of the two models under various biomechanical conditions were compared, and they were also compared with the Cage+BPS model in the literature.

The research results showed that in the Cage maximum Von-Mises stress and the maximum Von-Mises stress of the nail-rod system, the TLIF surgery model with implantation of fusion device 2 was significantly lower than the model with implantation of fusion device 1 and the Cage+BPS model in the literature; although the TLIF surgery model with implantation of fusion device 2 increased the maximum Von-Mises stress of the lower endplate of the fused segment, its value was still much lower than the yield stress of the L4 upper endplate. Through analysis, it can be concluded that the biomechanical characteristics of fusion device 2 are superior to those of fusion device 1 and the fusion devices in the Cage+BPS model.

Prospects

1) This study was based on the modeling of the lumbar spine data of a single healthy male volunteer and did not consider individual anatomical differences during the postoperative bone fusion process.
2) This study only conducted static analysis. Vibration analysis and fatigue performance tests can be carried out in the future.
3) This study only discussed the mechanical effect of applying this fusion device to a single segment. Further research can be conducted on the application of multi-segment fixation systems to provide more surgical options for spinal diseases in clinical practice.

References

[1] Zhang S, Liu W. Research on the Treatment of Lumbar Degenerative Diseases with Lumbar Intervertebral Fusion Device [J]. Practical Medical Research, 2024, 2(5). https://doi.org/10.70711/PMR.V2I5.6724

[2] Hu B, Li S Y. Comparison of Percutaneous Endoscopic-Assisted Lumbar Intervertebral Fusion Surgery and Traditional Surgical Approaches in the Treatment of Degenerative Lumbar Spondylolisthesis [J]. Medical Information, 2022, 35(10): 130-133. (in Chinese) https://doi.org/10.3969/j.issn.1006-1959.2022.10.031

[3] Schwender J D, Holly L T, Rouben D P, et al. Minimally invasive transforaminal lumbar interbody fusion (TLIF): technical feasibility and initial results [J]. Journal of Spinal Disorders & Techniques, 2005, 18 Suppl: S1-6. https://doi.org/10.1097/01.bsd.0000132291.50455.d0

[4] Wu M H, Li J, Zhang M X, et al. Efficacy and radiographic analysis of oblique lumbar interbody fusion for degenerative lumbar spondylolisthesis [J]. Journal of orthopaedic surgery and research, 2019, 14(1): 399. https://doi.org/10.1186/s13018-019-1416-2

[5] Malik A H, Kiebler A, Müller J, et al. Longitudinal analysis of radiological parameters after monosegmental lumbar instrumentation and posterior lumbar interbody fusion (PLIF) compared with transforaminal lumbar interbody fusion (TLIF) [J]. Journal of Orthopaedics, 2025, 69162-171. https://doi.org/10.1016/J.JOR.2025.06.002

[6] Tippins P N, Foreit M A, Kussow J N, et al. Examination of clinical and radiographic outcomes after lumbar interbody fusion: a retrospective analysis of TLIF, MidLIF, and MIS-TLIF procedures. [J]. Journal of Neurosurgery. Spine, 2025, 11-11. https://doi.org/10.3171/2025.1.SPINE241286

[7] Lv Q B, Gao X, Pan X X, et al. Biomechanical properties of novel transpedicular transdiscal screw fixation with interbody arthrodesis technique in lumbar spine: a finite element study [J]. Journal of Orthopaedic Translation, 2018, 15: 50-58. https://doi.org/10.1016/j.jot.2018.08.005

[8] Zhang G T, Wang Y, Zhang Z D, et al. Improved minimally invasive transforaminal lumbar interbody fusion for the treatment of degenerative lumbar diseases [J/OL]. Journal of Molecular Imaging, 2025, 48(04): 459-465. (in Chinese) https://doi.org/10.12122/j.issn.1674-4500.2025.04.11

[9] Chen L X. Finite element analysis of lumbar biomechanics after interbody fusion and bilateral transpedicular transdisc screw implantation [D]. Southwest Medical University, 2023. (in Chinese) https://doi.org/10.27215/d.cnki.glzyu.2023.000160

[10] Li M B, Huang Y B, Ren D C, et al. Finite Element Analysis of Three Different Lumbar Internal Fixation Fusion Methods [J]. Journal of Shandong University (Medical Edition), 2022, 60(01): 55-64. (in Chinese) https://doi.org/10.6040/j.issn.1671-7554.0.2021.0609

[11] Ma T, Li X, Wei Y J, et al. The influence of lateral nail rod position on segmental mobility, internal fixation, and cage stress in oblique lateral lumbar interbody fusion [J]. Chinese tissue engineering research, 2025, 29(33): 7165-7172. (in Chinese) https://doi.org/10.12307/2025.847

[12] Guo L X, Zhang C. Development and validation of a whole human body finite element model with detailed lumbar spine [J]. World Neurosurgery, 2022, 163: 579-592. https://doi.org/10.1016/j.wneu.2022.04.037

[13] Kahaer A, Zhang R, Wang Y, et al. Hybrid pedicle screw and modified cortical bone trajectory technique in transforaminal lumbar interbody fusion at L4-L5 segment: finite element analysis [J]. BMC Musculoskeletal Disorders, 2023, 24(1): 288. https://doi.org/10.1186/s12891-023-06385-y

[14] Hang Kai S, Yuru C, Zhenhua L, et al. Biomechanical evaluation of anterior lumbar interbody fusion with various fixation options: Finite element analysis of static and vibration conditions [J]. Clinical Biomechanics, 2021, 84: 105339-105339. https://doi.org/10.1016/j.clinbiomech.2021.105339

[15] Chong E, Pelletier M H, Mobbs R J, et al. The design evolution of interbody cages in anterior cervical discectomy and fusion: a systematic review. [J]. BMC Musculoskeletal Disorders, 2015, 16(1): 99. https://doi.org/10.1186/s12891-015-0546-x

[16] Zhao B R, Zheng X J, Ma J R. Research and Progress on Intervertebral Fusion Devices and Their Materials [J]. Tissue Engineering Research in China, 2017, 21(02): 315-321. (in Chinese) https://doi.org/10.1007/s10856-021-06609-4

[17] Li H Y. Establishment and effectiveness verification of delirium prediction model after posterior lumbar interbody fusion. [D]. Guizhou Medical University, 2024. (in Chinese) https://doi.org/10.27045/d.cnki.ggyyc.2024.000363

[18] Qiaolin Z, TeoEe C, Yan Z, et al. Finite element analysis of the lumbar spine in adolescent idiopathic scoliosis subjected to different loads. [J]. Computers in biology and medicine, 2021, 136 104745-104745. https://doi.org/10.1016/j.compbiomed.2021.104745

[19] Yang M J, Zeng C, Li L J, et al. Three-dimensional finite element modeling and analysis of lumbar interbody fusion surgery outside the intervertebral foramen [J]. Journal of Tongji University (Medical Edition), 2018, 39(03): 41-47. (in Chinese) https://doi.org/10.16118/j.1008-0392.2018.03.008

[20] Xu Z C, Wei B, Yang H S, et al. The application prospects and value of finite element modeling in lumbar spondylolysis [J]. Chinese tissue engineering research, 2018, 22(11): 1768-1773. (in Chinese) https://doi.org/10.3969/j.issn.2095-4344.0177

[21] Yamamoto I, Panjabi M M, Crisco T, et al. Three-dimensional movements of the whole lumbar spine and lumbosacral joint [J]. Spine, 1989, 14(11): 1256-1260. https://doi.org/10.1097/00007632-198911000-00020

[22] Chen C-S, Cheng C-K, Liu C-L, et al. Stress analysis of the disc adjacent to interbody fusion in the lumbar spine. [J]. Medical Engineering & Physics, 2001, 23(7): 485-493. https://doi.org/10.1016/S1350-4533(01)00076-5

[23] Sharma A, Sharma M D, Sehgal R. Experimental study of machining characteristics of titanium alloy (Ti–6Al–4V) [J]. Arabian Journal for Science and Engineering, 2013, 38(11): 3201-3209. https://doi.org/10.1007/s13369-012-0451-7

[24] Belwanshi M, Jayaswal P, Aherwar A. Mechanical behaviour investigation of PEEK coated titanium alloys for hip arthroplasty using finite element analysis [J]. Materials Today: Proceedings, 2022, 56: 2808-2817. https://doi.org/10.1016/j.matpr.2021.10.112

[25] Zhang Z, Fogel R G, Liao Z, et al. Biomechanical Analysis of Lateral Lumbar Interbody Fusion Constructs with Various Fixation Options: Based on a Validated Finite Element Model [J]. World Neurosurgery, 2018, 114 e1120-e1129. https://doi.org/10.1016/j.wneu.2018.03.158

[26] Wu Y, Loaiza J, Banerji R, et al. Structure-function relationships of the human vertebral endplate [J]. JOR Spine, 2021, 4(3): e1170. https://doi.org/10.1002/jsp2.1170